Interdependence of Parasitic Losses in Photonic Crystal Surface Emitting Lasers

Jingzhao Liu[1*], Xingyu Zhao[1], Zijun Bian[2], Paul Harvey[2], Scott Watson[1], Stephen. J. Sweeney[1], and Richard Hogg[3]

[1] *James Watt School of Engineering, University of Glasgow, Glasgow, G12 8QQ, United Kingdom*
[2] *School of Computing Science, University of Glasgow, Glasgow, G12 8QQ, United Kingdom*
[3] *Aston Institute for Photonic Technologies, Aston University, Aston Street, Birmingham, B4 7ET, United Kingdom*
[*] *j.liu.8@research.gla.ac.uk*

Abstract: It is common practice to use an un-pumped, PC containing region of a PCSEL to reduce in-plane optical power loss. We simulate the effect of self-absorption in this un-pumped region on the parasitic losses. It is found that the in-plane loss may be zeroed for a suitably thick un-pumped PC region width. However, in such devices the internal loss no longer has a unique value, and the dependence of the minimum total parasitic loss on a range of parameters is discussed.

Semiconductor lasers play an important role in a wide range of applications, such as data and telecommunication and optical storage due to their outstanding brightness characteristics and low cost of ownership [1-2]. Recently, photonic-crystal surface-emitting lasers (PCSELs) have gained significant interest due their high-quality, very-narrow-divergence and symmetric beam operation [3-4]. However, the characterisation of macroscopic device parameters for PCSELs is in its infancy, and suitable tools and understanding are required for, e.g. the optimisation of power conversion efficiency, or minimisation of threshold current, through e.g. the determination of different loss parameters [4-5].

The equations for slope efficiency (η_{SE}), and threshold gain (g_{th}) are [6]:

$$\eta_{SE} = \eta_i(1-A)\frac{h\nu}{q}\frac{\frac{1}{2}\left(1+2\sqrt{R}Cos\theta+R\right)\alpha_{rad}}{\left(1+\sqrt{R}Cos\theta\right)\alpha_{rad}+\alpha_{//}+\alpha_i} \quad (1)$$

$$g_{th} = \left(1+\sqrt{R}Cos\theta\right)\alpha_{rad}+\alpha_{//}+\alpha_i \quad (2)$$

where η_i is internal quantum efficiency, A is due to absorption in the substrate, R is the reflectivity of the vertical DBR mirror. θ is the phase between upward-radiated and reflected light. α_{rad} is radiation constant, $\alpha_{//}$ is the in-plane optical loss, and α_i is the internal loss. By contrast to other classes of laser, there is an additional loss term due to in-plane loss ($\alpha_{//}$) of optical power to regions without photonic crystal (PC) structures ~~that can scatter vertically~~, and this loss term (optical power exiting the PC patterned region) is the focus of this report.

It is a commonly used technique to reduce $\alpha_{//}$ in PCSELs by having a PC region larger than the laser contact region and that the internal loss α_i is both constant and dominated by free-carrier absorption [5, 7]. However, the effect of self-absorption of light by the un-pumped active region has not been considered. Here we address this gap in knowledge, with a view to providing design guidelines to enhance the power conversion of PCSELs.

In this paper we report on the simulation of large, finite size PCSEL devices to explore the effects of an un-pumped PC containing perimeter on total losses, using a probabilistic Markov chain model [8]. Our model considers electrically pumped devices, but is applicable to optically pumped devices. We show that if the un-pumped perimeter does not

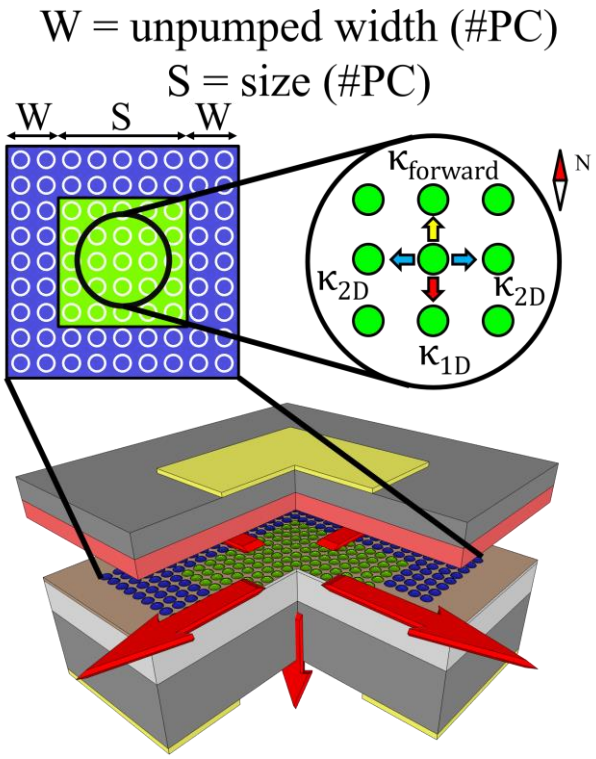

Figure 1: Schematic of a substrate-emission PCSEL device showing the pumped and un-pumped PC region. Red arrows represent the macroscopic, device level power loss mechanisms. The plan view of PC matrix sows W is width of un-pumped region, and S is the size of pumped region. The microscopic light scattering mechanism of PCSEL are also shown.

include any additional power loss (e.g. self-absorption) then α_i is well defined and that $\alpha_{//}$ may be effectively zeroed by making the perimeter suitably wide. However, once we include self-absorption by the un-pumped active element, we find that both parasitic loss terms ($\alpha_{//}$ and α_i) are linked, and total parasitic loss ($\alpha_{//}+\alpha_i$) is a function of both perimeter width and QW absorption (QW number and PCSEL operating wavelength). We then analyze this minimum total parasitic loss as a function of perimeter width, QW number, and gain-peak/PCSEL wavelength detuning. These results provide new insight into unlocking methods to assess PCSEL devices and indicate that to enhance photonic crystal efficiency in current devices, a non-absorbing PC containing perimeter should be introduced.

Figure 1 shows a schematic of a substrate emission PCSEL device, illustrating the device simulated, where the PC grating region is larger than the p-contact. Here a square contact [9-12] is adopted, although arbitrarily shaped structures can be readily accommodated such as circular contacts [13-15]. S indicates the lateral size of the pumped region of the PC atom matrix, and W is the width of the un-pumped region. We use the number of PC atoms as a dimensionless value. The zoomed in image shows other inputs for probabilistic Markov chain model. We convert cm^{-1} values to realize probabilities for optical power scattering at each PC atom; κ_{1D} is the probability of scattering 180°; κ_{2D} of scattering in-plane by 90°; κ_{rad} is the probability of scattering vertically, and κ_i is the probability of internal loss (not shown in the figure); $\kappa_{forward}$ of the photon keeping the original direction and defined as:

$$\kappa_{forward} = 1 - \kappa_{1D} - 2 \times \kappa_{2D} - \kappa_{rad} - \kappa_i \qquad (3)$$

Here, scattering into other in-plane directions (e.g. Γ-M or modes from other bands) is accommodated within these scattering coefficients. For example, for TE waves and a square lattice κ_{2D} results from multiple higher order scattering, and

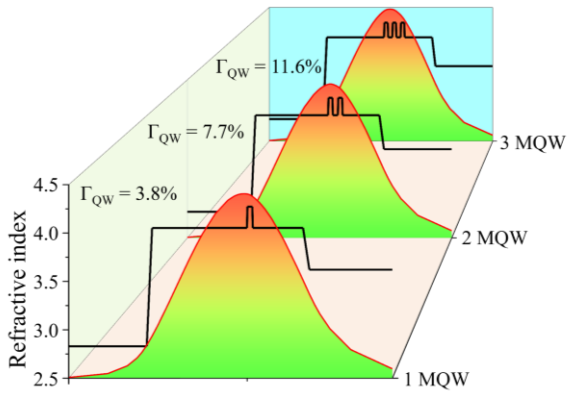

Figure 2: Schematic of the mode-profile of the simulated PCSEL device [7] as a function of MQW number. Confinement factor, Γ_{QW}, (overlap of the MQW and mode) is shown for each case.

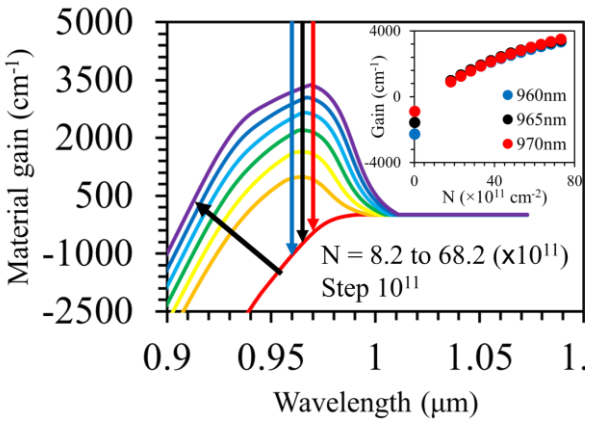

Figure 3: Calculated material gain spectrum for InGaAs/AlGaAs quantum well at room temperature as a function of carrier density. Inset shows the material gain at three operating wavelengths as a function of carrier density and the zero-carrier absorption.

scattering into other modes would appear as a power loss in κ_i.

We consider a 940nm PCSEL [7] for our input parameters. Coupling coefficients were extracted from the band-structure, and structural information [7& 16] allows waveguide modelling. Following convergence [8 & 17], we are able to extract macroscopic values for radiative α_{rad}, in-plane $\alpha_{//}$ and internal loss α_i.

Figure 2 shows a schematic showing the simulated mode-overlap for a single, double, and triple QW active element using reported core, cladding and PC structures (details in Supplementary) [7]. The QW confinement factors, MQW, for one, two and three MQW are 3.8%, 7.7% and 11.6%, respectively. This follows an almost linear relationship, as expected for low QW number [18].

Figure 3 shows the simulated material gain of the simulated

PCSEL Wavelength (nm)	Material Gain (cm^{-1})	Quantum Well Absorption (cm^{-1})		
QW Number		1	2	3
970	-917	-35	-70	-106
965	-1602	-61	-123	-185
960	-2270	-87	-174	-262

Table 1: Quantum well absorption coefficients in the un-pumped perimeter region at three PCSEL operating wavelengths as a function of quantum well number.

devices as a function of carrier density. The simulation is based on an 8x8 KP band structure calculation for TE Polarization QW. Three wavelengths are compared, corresponding to the gain-spectrum peak at 965nm (black arrow), and blue and red arrow (± 5nm detuning). The inset to figure 3 shows

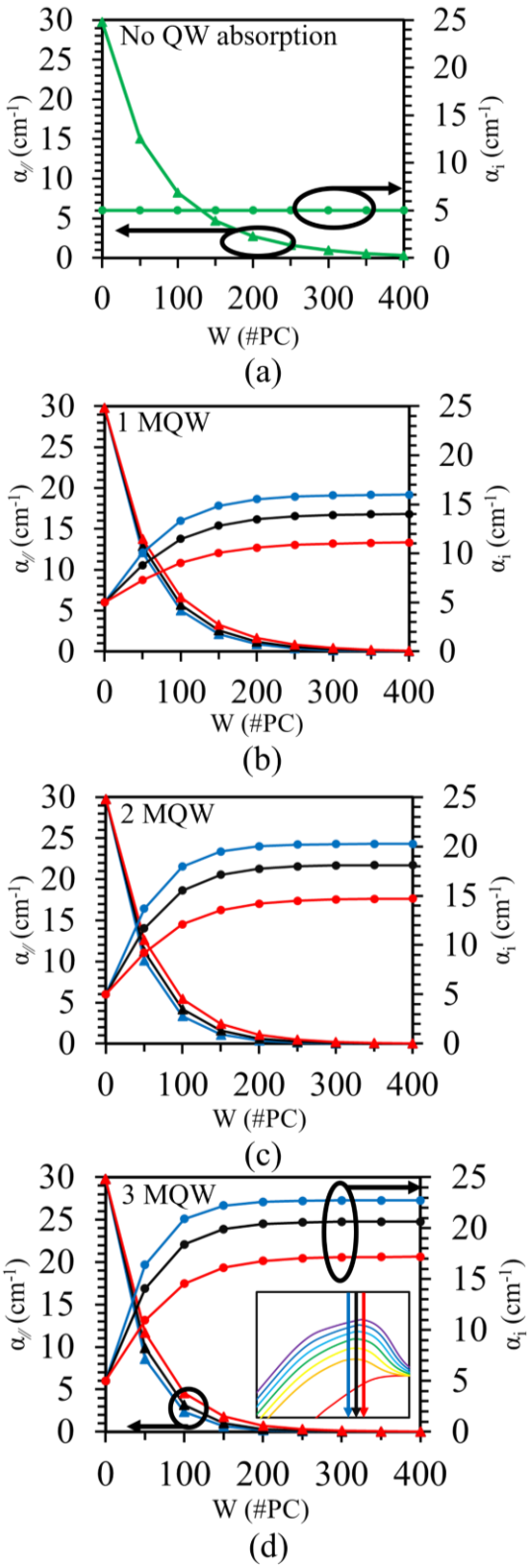

Figure 4: Simulated in-plane and internal loss as a function of un-pumped perimeter PCSEL width W, for (a) no QW absorption, (b) 1 QW, (c) 2 QW, (d) 3 QW. Values are determined using different PCSEL operating wavelengths (960nm, 965nm, 970nm) as shown in the inset to (d).

the modal gain at these three wavelengths. We extract the absorption loss for use in further simulations as shown in table 1.

To complete the input parameters for the simulation, the out-of-plane loss (α_{rad}) is assumed as constant (38 cm^{-1}). [7] The PCSEL pumped area in the simulation has fixed size (700 x 700 PC atoms), and the un-pumped region width is varied. The in-plane loss ($\alpha_{//}$) and internal loss (α_i) from probabilistic Markov chain modeling for free carrier loss both alone and as a function of additional MQW absorption in Figure 4. Our probabilistic Markov chain simulations do not consider absorption bleaching.

Figure 4 plots the in-plane and internal loss as a function of the width of the un-pumped region W considering (a) only internal loss α_i, (b) self-absorption of 1 QW, (c) self-absorption of 2 QWs, and (d) self-absorption of 3 QWs.

For the case where there is no self-absorption, (Fig 4(a)), as the un-pumped region width is increased, in-plane loss tends towards zero, and internal loss remains a constant value. For the values of in-plane coupling used here (supplementary material) this zeroing of in-plane loss occurs at around W=400. With the introduction of self-absorption for 1 QW in the un-pumped gain region (Fig 4(b)) we observe an increase in α_i with increasing W, and a corresponding reduction in $\alpha_{//}$. As W is increased, more light is lost to self-absorption and internal loss increases. This increase is a function of detuning of the lasing peak to the gain-spectrum peak (and hence un-pumped QW absorption). Here, the in-plane loss is essentially zeroed at W=350. Beyond W=350, α_i reaches a constant value that is a function of the detuning of the PCSEL wavelength and the gain-spectrum peak. This demonstrates an interdependence between $\alpha_{//}$ and α_i in the case of a PCSEL with un-pumped boundary PC. The effect of introducing more QWs is to reduce the thickness of the boundary PC at which $\alpha_{//}$ is zeroed, but the constant value of α_i at this point is higher.

The effect of current spreading may be invoked to suggest that the boundary region does not exhibit the levels of loss shown in table 1. Simulation of the current spreading is shown in Supplementary (figure S1) and indicates a ~50% reduction in carrier density is predicted over ~10 #PC. This compares to length scales of 250-400 #PC required to zero $\alpha_{//}$. The inclusion of absorption bleaching at high in-plane powers will modify the situation a little, with bleached regions close to the contact having only free-carrier loss, and more peripheral regions being un-bleached. Its inclusion will not remove the inter-dependency of the parasitic loss parameters. We note that if practically relevant, an increase in slope efficiency with increasing power would be observed in devices that include an un-pumped perimeter, and this is not the case.

The input parameters used in Hirose *et al.* [7] indicate an absorption coefficient of ~150 cm^{-1} in the unpumped boundary

PC region in order to agree with the slope efficiency described therein. Similar absorption coefficients provide agreement to the slope efficiency from Yoshida *et al.*, using the input microscopic scattering parameters they supply. Our work suggests that a detailed experimental study, varying gain peak – operating wavelength detuning, QW number, is now required.

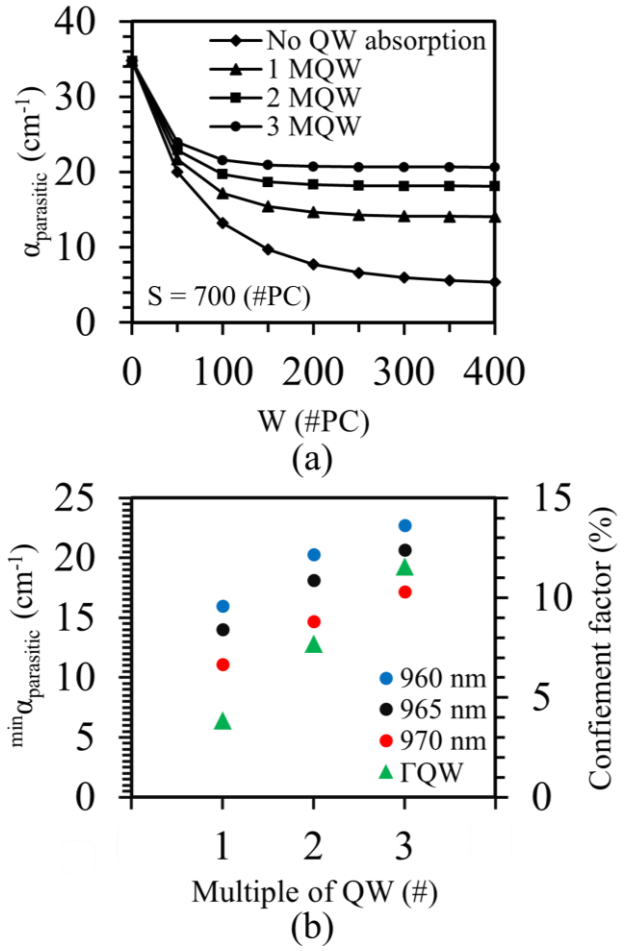

Figure 5: (a) Total parasitic loss as a function of un-pumped region W for different QW number (including intrinsic loss alone) for the three PCSEL operating wavelengths. (b) Minimum parasitic loss and confinement factor as a function of different QW number for the three PCSEL operating wavelengths.

The parasitic loss ($\alpha_{parasitic}$) is defined as the sum of the in-plane loss and internal loss ($\alpha_{parasitic} = \alpha_{//}+\alpha_i$) and is plotted as a function of un-pumped PC number in Figure 5(a). We plot data for perfect alignment of the PCSEL emission and gain-spectrum peak for clarity. It shows the decreasing trend of parasitic loss with increasing W. The parasitic loss will be minimized by increasing W, but the internal loss and in-plane loss are inter-related. For large W, where $\alpha_{//}$ is zeroed, total parasitic loss is dominated by α_i, and reaches a minimum value($^{min}\alpha_{parasitic}$). Increasing MQW number increases the parasitic loss as the fraction of light lost radiatively in the un-pumped region reduces, due to the competing power loss channels in self-absorption.

Figure 5(b) plots the minimum parasitic loss as a function of QW number and lasing wavelength detuning to the gain-spectrum peak. We also plot the QW confinement factor as a function of MQW number for reference and note the strong correlation between QW overlap and minimum parasitic loss.

We have reported the simulation of the effects of self-absorption on the device-level losses of large, finite size PCSEs that incorporate an un-pumped boundary PC layer. This is achieved by the incorporation of QW absorption in a probabilistic Markov chain model. We find that the introduction of self-absorption due to the un-pumped QW region results in the parasitic losses α_i and $\alpha_{//}$ becoming interdependent. In this case, α_i is no longer a constant, but is a function of QW number, W and operating wavelength (detuning to gain-spectrum peak leads to different QW absorption coefficient). Beyond certain W, α_i reaches a maximal value, and $\alpha_{//}$ can be effectively zeroed. Total parasitic loss is shown to reach a minimum value once W is sufficient to zero in-plane loss, and the value is correlated to the QW confinement factor and operating wavelength. These results indicate that technologies that remove this self-absorption may be required to improve future power conversion efficiency of the PCSEL.

Supplementary Materials

Additional simulation of current spreading is provided as supplementary data.

Acknowledgements

This work was supported by EP/X032868/1; Integrated Solid-State Steerable Lasers (I-STEER)

References

[1] S. Kumar and M. J. Deen, Fiber Optic Communications. Chichester, UK: John Wiley & Sons, Ltd, apr 2014.

[2] R. Alan. Essentials of Optoelectronics with applications. Vol. 4. CRC Press, 1997.

[3] Peng, Chun-Yen, et al. "Performance analyses of photonic-crystal surface-emitting laser: Toward high-speed optical communication." Nanoscale Research Letters 17.1 (2022): 90.

[4] M. Yoshida, et al., 2021 J. Phys. Photonics 3 022006

[5] S. Noda, et al., "High-power and high-beam-quality photonic-crystal surface-emitting lasers: a tutorial," Adv. Opt. Photon. 15, 977-1032 (2023)

[6] Y. Itoh, et al., "High-power and high-efficiency operation of 1.3 μm-wavelength InP-based photonic-crystal surface-emitting lasers with metal reflector," Opt. Express 32, 12520-12527 (2024)

[7] K. Hirose, et al., "Watt-class high-power, high-beam-quality photonic-crystal lasers". Nature Photon 8, 406–411 (2014). https://doi.org/10.1038/nphoton.2014.75

[8] J. Liu, et al., Probabilistic Markov chain modeling of photonic crystal surface emitting lasers. Appl. Phys. Lett. 25 December

2023; 123 (26): 261107. https://doi.org/10.1063/5.0168073 (See https://github.com/Jingzhao-Liu/Probabilistic-Markov-Chains-Modelling Quarter for “Probabilistic-Markov-Chains-Modelling-(Quarter version).”)

[9] Z. Bian, et al., “Resonator embedded photonic crystal surface emitting lasers”. npj Nanophoton. 1, 13 (2024). https://doi.org/10.1038/s44310-024-00014-9

[10] Y. Liang, et al., “Room temperature surface emission on large-area photonic crystal quantum cascade lasers”. Appl. Phys. Lett. 21 January 2019; 114 (3): 031102. https://doi.org/10.1063/1.5082279

[11] I. Takuya. et al., "Comprehensive analysis of photonic-crystal surface-emitting lasers via time-dependent three-dimensional coupled-wave theory." Physical Review B 99.3 (2019): 035308.

[12] Z. Bian et al., "1.5 μm Epitaxially Regrown Photonic Crystal Surface Emitting Laser Diode," in IEEE Photonics Technology Letters, vol. 32, no. 24, pp. 1531-1534, 15 Dec.15, 2020, doi: 10.1109/LPT.2020.3039059.

[13] Wang, Z., Liu, X., Wang, P. et al., “Continuous-wave operation of 1550 nm low-threshold triple-lattice photonic-crystal surface-emitting lasers”. Light Sci Appl 13, 44 (2024). https://doi.org/10.1038/s41377-024-01387-4

[14] C. -J. Chang. et al., "High Power Short Wavelength Infrared Photonic Crystal Surface Emitting Lasers," in Journal of Lightwave Technology, vol. 42, no. 15, pp. 5262-5268, 1 Aug.1, 2024, doi: 10.1109/JLT.2024.3390989.

[15] Morita, R., Inoue, T., De Zoysa, M. et al., Photonic-crystal lasers with two-dimensionally arranged gain and loss sections for high-peak-power short-pulse operation. Nat. Photonics 15, 311–318 (2021). https://doi.org/10.1038/s41566-021-00771-5

[16] K. Sakai, E. Miyai, and S. Noda, "Coupled-wave model for square-lattice two-dimensional photonic crystal with transverse-electric-like mode", Appl. Phys. Lett. 89, 021101 (2006) https://doi.org/10.1063/1.2220057

[17] J. Liu. et al., "Convergence criteria for probabilistic Markov chains modelling of photonic crystal surface emitting lasers," Proc. SPIE 12440, Novel In-Plane Semiconductor Lasers XXII, 124400D (15 March 2023); https://doi.org/10.1117/12.2649077

[18] P. M. Ilroy, A. Kurobe and Y. Uematsu, "Analysis and application of theoretical gain curves to the design of multi-quantum-well lasers," in IEEE Journal of Quantum Electronics, vol. 21, no. 12, pp. 1958-1963, December 1985, doi: 10.1109/JQE.1985.1072606.